Fe-catalyzed sulfide oxidation in hydrothermal plumes is a source of reactive oxygen species to the ocean

Timothy J. Shaw[a,1], George W. Luther III[b], Richard Rosas[b,2], Véronique E. Oldham[b,3], Nicole R. Coffey[b,4], John L. Ferry[a], Dewamunnage M. C. Dias[a], Mustafa Yücel[c], and Aubin Thibault de Chanvalon[b,5]

[a]Department of Chemistry and Biochemistry, University of South Carolina, Columbia, SC 29208; [b]School of Marine Science and Policy, University of Delaware, Lewes, DE 19958; and [c]Institute of Marine Sciences, Middle East Technical University, 33731 Mersin, Turkey

Edited by Ellen R. M. Druffel, University of California, Irvine, CA, and approved August 19, 2021 (received for review December 28, 2020)

Historically, the production of reactive oxygen species (ROS) in the ocean has been attributed to photochemical and biochemical reactions. However, hydrothermal vents emit globally significant inventories of reduced Fe and S species that should react rapidly with oxygen in bottom water and serve as a heretofore unmeasured source of ROS. Here, we show that the Fe-catalyzed oxidation of reduced sulfur species in hydrothermal vent plumes in the deep oceans supported the abiotic formation of ROS at concentrations 20 to 100 times higher than the average for photoproduced ROS in surface waters. ROS (measured as hydrogen peroxide) were determined in hydrothermal plumes and seeps during a series of *Alvin* dives at the North East Pacific Rise. Hydrogen peroxide inventories in emerging plumes were maintained at levels proportional to the oxygen introduced by mixing with bottom water. Fenton chemistry predicts the production of hydroxyl radical under plume conditions through the reaction of hydrogen peroxide with the abundant reduced Fe in hydrothermal plumes. A model of the hydroxyl radical fate under plume conditions supports the role of plume ROS in the alteration of refractory organic molecules in seawater. The ocean's volume circulates through hydrothermal plumes on timescales similar to the age of refractory dissolved organic carbon. Thus, plume-generated ROS can initiate reactions that may affect global ocean carbon inventories.

superoxide | HO | carbon cycle | hydrogen peroxide | sulfide oxidation catalysis

The reduction of dioxygen by ferrous complexes is the initiating step for a chain of reactions (Eqs. **1**–**3**) that is among the most important sources of reactive oxygen species (ROS) in the aquatic environment (1). ROS are a class of powerful oxidants that include the hydroperoxyl radical (HO_2) and its conjugate base (superoxide, O_2^-), hydrogen peroxide (H_2O_2), and hydroxyl radical (HO). Solar-induced photoprocesses with organic matter in freshwater and seawater are a major source of ROS (as O_2^-, H_2O_2, and HO) (2, 3). The inventory and production rates for H_2O_2 in surface seawater are the highest of the ROS (2). However, hydroxyl radical is the most reactive of the ROS and can rapidly oxidize most organic molecules (1, 3). The production of H_2O_2 can support the subsequent production of hydroxyl radical by the reaction of H_2O_2 with Fe(II) through Fenton and photo-Fenton reactions (1). This process creates a link between the carbon cycle and the sources of Fe(II) and H_2O_2 to oxygenated waters in the ocean (1).

The rate of the reaction between Fe(II) and H_2O_2 (Eq. **3**) at typical seawater pH values is competitive with the rates reported for the reaction of Fe(II) with O_2 (Eq. **1**) (4, 5). In contrast, the rates for photoproduction of hydroxyl radical via the photolysis of precursors are relatively slow (1). Thus, in surface seawater, the rate of photoproduction of Fe(II) is an important factor contributing to the intensity of hydroxyl radical production and the associated abiotic oxidation of organic carbon (1). However, Fe(II) is also produced by microbial processes in the oceans, including the action of facultative anaerobes, and is a critical intermediate in the catalytic oxidation of hydrogen sulfide by dioxygen (6, 7). Microbial processes at redox interfaces have been well established as sources of reductive equivalents that lead to ROS production, including O_2^- and H_2O_2 (6–8). While photoprocesses have generally been accepted as the more significant source of H_2O_2 and Fe(II), hydrothermal systems (vents and seeps) are major, direct sources of reduced Fe and S species to the oceans (9, 10). Given the kinetics of the Fenton process (1, 5), the venting of hydrothermal fluids should support a very high intensity of ROS production and organic carbon mineralization in hydrothermal plumes.

The reduction of Fe(III) by H_2S in the plumes and the corresponding abiotic oxidation of Fe(II) species [e.g., $Fe^{2+}_{(aq)}$, $FeS_{(s)}$] should maintain the ROS production cycle until the available reduced sulfur species have been oxidized (Eqs. **1**–**4**). The corresponding yield of ROS would be limited to the summed total of reductive equivalents injected by H_2S and Fe(II) species (Eq. **5**). This process would be analogous to that seen in coastal pore waters but not limited by the rate of microbial metabolism (6–8, 11). Superoxide, generated via Fe(II) oxidation, could then react with Fe(II) or Mn(II) to generate H_2O_2 (Eqs. **1**, **2**, and **6**) (8, 12). While Fe(II) in vent water should exist primarily as sulfide phases (e.g., FeS clusters), ambient Fe(III) can react catalytically with reduced S species (e.g., H_2S and FeS). These, in turn, can

Significance

The Fe-catalyzed oxidation of sulfide by dioxygen in hydrothermal vent plumes is shown to be a source of reactive oxygen species (ROS) to the deep ocean. ROS are a class of powerful oxidants, the most reactive of which can react with recalcitrant organic molecules at near diffusion limited rates. ROS production in hydrothermal systems may be comparable to the known photochemical yields of ROS in surface waters. The discovery of this abundant hydrothermal source of ROS demonstrates a mechanism for the alteration of refractory organic matter in the deep ocean.

Author contributions: T.J.S. designed research; T.J.S., G.W.L. III, R.R., V.E.O., N.R.C., D.M.C.D., M.Y., and A.T.d.C. performed research; T.J.S. contributed new reagents/analytic tools; T.J.S., G.W.L. III, and J.L.F. analyzed data; and T.J.S., G.W.L. III, and J.L.F. wrote the paper.

The authors declare no competing interest.

This article is a PNAS Direct Submission.

[1]To whom correspondence may be addressed. Email: shaw@mailbox.sc.edu.

[2]Present address: Department of Oceanography, Texas A&M University, College Station, TX 77843.

[3]Present address: Graduate School of Oceanography, University of Rhode Island, Narragansett, RI 02882.

[4]Present address: College of Earth, Ocean, and Atmospheric Sciences, Oregon State University, Corvallis, OR 97331.

[5]Present address: CNRS, Institute of Analytical Sciences and Physical-Chemistry for the Environment and Materials, 5254 Pau, France.

This article contains supporting information online at https://www.pnas.org/lookup/suppl/doi:10.1073/pnas.2026654118/-/DCSupplemental.

Published September 30, 2021.

regenerate Fe(II) and maintain the ROS production chain (Eq. **4**), as long as reduced S species are available (12). Similarly, some of the produced superoxide can react with ambient Fe(III) and regenerate Fe(II) (the back reaction in Eq. **1**) and still maintain the ROS production cycle. The physiochemical processes leading to these unique reaction mixtures are depicted conceptually in Fig. 1, and the measured reactants and products are presented in Table 1. The maintenance of the Fe cycle by reduced S species can also support a chain reaction, resulting in additional ROS production including hydroxyl radical (1, 6, 7). Hydroxyl radical can readily react with refractory molecules that are kinetically inhibited from direct reaction with O_2 (13).

The potential scale of ROS production in hydrothermal plumes is a function of the flux of reduced sulfur species from vents and the bottom-water O_2 that mixes within the plume (Eq. **5**) to maintain the Fe(II)/Fe(III) cycle (9, 10, 14–17). As noted above, Fe(II) and/or reduced sulfur species are typically the limiting reactants in seawater. The hypothesis tested here is that O_2 is the limiting reagent during the initial mixing of hydrothermal vent waters with ambient seawater to form the plume.

$$\mathrm{Fe(II)_{tot}} + \mathrm{O_2} \leftrightarrow \mathrm{Fe(III)} + \mathrm{O_2^-}\ (\text{oxygen reduction}), \qquad [1]$$

$$\mathrm{Fe(II)_{tot}} + \mathrm{O_2^-} + 2\,\mathrm{H^+} \rightarrow \mathrm{Fe(III)} + \mathrm{H_2O_2}\ (\text{superoxide reduction}), \qquad [2]$$

$$\mathrm{Fe(II)} + \mathrm{H_2O_2} + \mathrm{H^+} \rightarrow \mathrm{Fe(III)} + \mathrm{H_2O} + \mathrm{HO\bullet}\ (\text{Fenton reaction}), \qquad [3]$$

$$2\,\mathrm{Fe(III)} + \mathrm{H_2S} \rightarrow 2\,\mathrm{Fe^{2+}} + \mathrm{S^0} + 2\,\mathrm{H^+}\ (\text{sulfide oxidation sustained Fe(II) regeneration}), \qquad [4]$$

$$\mathrm{O_2} + \mathrm{H_2S} \rightarrow \mathrm{S^0} + \mathrm{H_2O_2}\ (\text{sulfide induced ROS formation as the sum of Eqs. 1, 2, and 4}), \qquad [5]$$

$$\mathrm{Mn(II)_{tot}} + \mathrm{O_2^-} + 2\,\mathrm{H^+} \rightarrow \mathrm{Mn(III)} + \mathrm{H_2O_2}\ (\text{Mn(II) oxidation}). \qquad [6]$$

Accepting that the plume inventory of H_2S can maintain the Fe cycle (Eq. **4**), then sulfide oxidation in the plume would set an upper limit on ROS production arising from the vent flux of reduced Fe and S species (Eq. **5**) (6, 7). Eq. **5** shows the expected reaction chain intermediate, H_2O_2, resulting from the net cycle of metal-mediated H_2S oxidation as the sum of reactions depicted in Eqs. **1**, **2**, and **4**. Fig. 2 depicts the intersection of the Fe and S oxidation cycles with the full ROS reaction chain in plumes. The cycles include pathways for ROS-mediated reactions with dissolved organic carbon (DOC) that lead to hydroxylated aromatic and aliphatic organic molecules in vent systems (18). Hydrogen peroxide is a relatively long-lived intermediate in the ROS reaction chain depicted having a half-life of days in seawater where Fe(II) species are limiting (6, 19). Hydrogen peroxide was selected as an ROS production indicator for this study because it is the rate-limiting intermediate between the very short-lived ROS in the reaction chain, superoxide and hydroxyl radical. The proposed ROS production cycle was investigated by measurement of a suite of reactants and products in plume waters using a series of samplers and sensors deployed from the human occupied submersible *Alvin*, at 9° 50′ North East Pacific Rise (EPR).

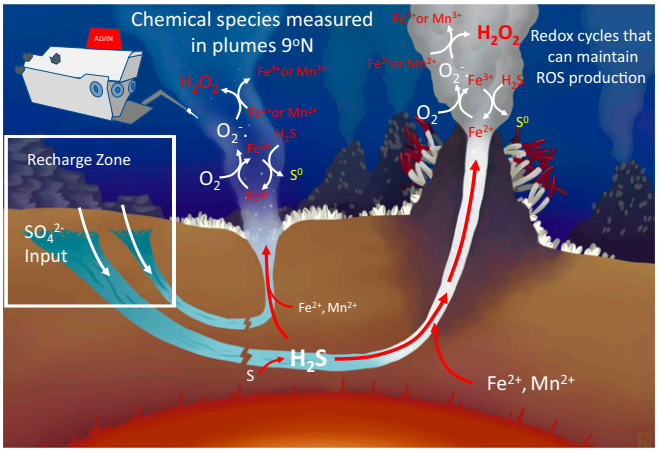

Fig. 1. Conceptual view of the entrainment of oxygenated bottom water into plumes and the resultant generation of ROS as vent-derived species react with ambient seawater. Image credit: Kathryn Shaw (artist).

Results

ROS Production in Vent Plumes. H_2O_2 was measured on samples from three different *Alvin* dives (Table 1). One sample reference set was collected in the deep-water column for comparative purposes and two at vent locations, low-temperature Q-vent and high-temperature Biovent at 9° N. The amplex red technique was employed to measure hydrogen peroxide in the samples in situ (20). Syringe samplers (modified from ref. 21) were precharged with amplex red and horseradish peroxidase (HRP) in a phosphate buffer and deployed in the *Alvin* equipment basket. Samples were drawn through a Teflon sipper tube into the syringes where H_2O_2 drove the conversion of amplex red to the stable product resorufin, which was visible in syringes immediately upon collection. The concentration of resorufin was later measured fluorometrically upon return to the ship (20).

All samples from vent-affected waters (within plumes or associated diffuse flow fields) showed statistically significant (relative to background) hydrogen peroxide concentrations ranging from 1.1 to 6.2 μM. Reference deep-water samples, collected away from vent-affected waters, did not contain statistically significant amounts of hydrogen peroxide relative to blanks (≤ 200 nM; see *Materials and Methods*). When possible, syringe samples without reagents were also collected from the same position in plumes for determination of ambient Fe and Mn species. Fe(II) and Mn(II) were present in every plume sample collected. Mn(III) was detected in several plume samples but Fe(III) was not. The sipper used for H_2O_2, Fe, and Mn sample collection was attached to an electrochemical probe that provided measurements of O_2 and sulfide phases in situ by cyclic voltammetry (22). In most cases, voltammetric measurements were taken synoptically with the discrete syringe sampling. Temperature limitations on the probe precluded sampling near the high-temperature vent fluid endmembers (e.g., 360 °C at biovent). However, separate discreet samples were collected with Ti samplers in the plumes, allowing the measurement of temperature, bromide, iodide, and additional sulfur species including S^0 at most sites and temperatures (23).

The concentration of reduced Fe(II) species in the plume samples correlated positively with temperature consistent with the input of reduced Fe species in the vent fluid (Fig. 3). The concentration of H_2O_2 correlated inversely with temperature in the plume for both vent locations (Fig. 3), and the regression indicated that H_2O_2 was not detectable above 39 °C. At high temperature, the direct reactions of H_2O_2 would be kinetically fast in the presence of excess Fe(II) and sulfide and support a very intense ROS production chain but limit the H_2O_2 inventory. The absence of detectable H_2O_2 in ambient reference bottom water (Table 1) precluded seawater mixing as a source for the high-plume H_2O_2 inventory. The increase in H_2O_2 as a function

Table 1. Dives and sample locations with physical and chemical parameters measured. Abbreviations used in the table are: Plume-xM= vent plume and approximate height above orifice; Free SH_2S = [H_2S] + [HS^-]

Dive No.	Location	T °C	O_2 μM observed	O_2 μM predicted	H_2O_2μM	Fe(II) μM	Mn(II) μM	Mn(III) μM	pH	Free ΣH_2S μM
4886 (n = 3)	Water Column	1.85	105	105	below detection limit	not measured	not measured	not measured	not measured	not measured
4888	Biovent Diffuse Flow	15.5	below detection limit	100	4.5	not measured	not measured	not measured	not measured	16.6
4888	Biovent Diffuse Flow	15.5	below detection limit	100	2.9	not measured	not measured	not measured	not measured	10.9
4888	Biovent Plume-1 m	9.5	below detection limit	102	2.9	not measured	not measured	not measured	not measured	5.79
4888	Q-Vent, Plume-3 m	6.0	10	94	5.2	49	21.4	3.93	not measured	45.8
4888	Q-Vent, Plume-<1m	9 to 11	below detection limit	82	4.7	not measured	not measured	not measured	not measured	31.2
4888	Q-Vent, Plume-1 m	2.0	80	105	6.2	21.2	9.75	below detection limit	not measured	32.9
4890	Biovent, Plume-<0.5 m	25 to 30	below detection limit	96	2.2	not measured	not measured	not measured	not measured	223
4890	Biovent, Plume-<0.5 m	27 to 30	below detection limit	97	2.8	289	4.75	10.2	6.60	250
4890	Biovent, Plume -1 m	5 to 9	below detection limit	102	5.8	8.30	8.96	7.69	6.28	72.6
4890	Q-Vent, Plume-<0.5 m	20 to 30	below detection limit	39	1.1	not measured	not measured	not measured	not measured	186
4890	Q-Vent, Plume-<0.5 m	20 to 30	below detection limit	39	2.3	273	100.3	below detection limit	5.42	81.8
4890	Q-Vent, Plume-1 m	7 to 8	below detection limit	87	6.2	134	49.8	6.14	5.81	below detection limit

of plume mixing with bottom water was consistent with ROS production during oxidation of reduced Fe species as depicted in Fig. 3. On cooling in the plume, further reactions of H_2O_2 were kinetically slower. As the plume aged and temperature decreased, Fe(II), sulfide, and other reductants were lower in concentration and led to a longer residence time of the H_2O_2 intermediate that was observed as a larger inventory.

Superoxide production was not measured directly due to matrix interferences in the plume and expected short lifetime (i.e., low concentration) under plume conditions. However, the presence of hydrogen peroxide alone was evidence for the production of superoxide, an essential intermediate for hydrogen peroxide production (12). Superoxide would not be expected to have a long lifetime in the plume environment given its reactivity with Fe(II) or Mn(II) (Eq. **6**, similar to Eq. **2**).

The one-electron oxidation of Mn(II) to Mn(III) by oxygen is thermodynamically unfavorable (12, 24), but the reaction of Mn(II) with superoxide is favorable and is rapid based on the rate constant for the Mn(II) reduction of superoxide to H_2O_2 ($k = 1 \times 10^8\ M^{-1} \cdot s^{-1}$ versus $1.5 \times 10^6\ M^{-1} \cdot s^{-1}$ for Fe(II)) (25). A number of plume samples taken in conjunction with H_2O_2 measurements had measurable levels of a stable complex of Mn(III) (Table 1). This observation indicated an abiotic mechanism for Mn(II) oxidation that was consistent with superoxide production in the plume. The result confirmed a chain reaction for ROS production initiated by the one-electron oxidation of Fe^{2+} with concurrent reduction of dioxygen to generate superoxide. Rapid reaction of superoxide with ambient Fe(II), Mn(II), and other reductants is likely to outcompete the back reaction of Eq. **1**, supporting the measured H_2O_2 inventory.

The progress of the proposed reaction chain was evident in the mixing zone at Q-vent. The temperature of the vent fluid at Q-vent (40 °C) allowed collection of samples through much of the mixing zone in the plume. Samples were collected from near the orifice (30 °C) up the plume to ∼1 m where the temperature change indicated rapid mixing with bottom water to yield a plume temperature near ambient (2 °C). Rapid mixing of bottom water carried dissolved O_2 into the plumes, yet O_2 was undetectable in 10 of the 12 samples where Fe^{2+} and H_2O_2 were collected and detected at the vent sites (Table 1), suggesting oxygen limitation during the initial plume formation. The hypothesis that oxygen reduction was proportional to H_2O_2 production, as predicted from the summed reactions presented as Eq. **5**, was tested using the Q-vent plume data. Temperature was used as a conservative tracer of mixing between vent and bottom-water endmembers to calculate the initial O_2 input during mixing. At Q-vent, the vent fluid endmember was 40 °C, and the oxygen was assumed to be zero. Bottom water was 1.6 °C, and oxygen was 105 μM. The predicted oxygen concentration at any point in the plume is the fraction of bottom water in the plume (F_b, Eq. **7**) multiplied by 105 μM (Table 1).

$$F_b = 1\text{-}\left((T_p\text{-}\,T_b)/(T_v\text{-}\,T_b)\right), \qquad [7]$$

where T_p was the plume temperature, T_b is the bottom-water temperature, and T_v was the vent fluid temperature. The fraction of bottom water (as percent) and predicted initial oxygen concentration (equivalent to O_2 consumed as O_2 measured was typically below the detection limit) were plotted against measured H_2O_2 for Q-vent (Fig. 4).

Discussion

The strong correlation between initial oxygen concentration and H_2O_2 (Fig. 4) suggested that O_2 was the limiting reactant (Eqs. **1** and **2**) during initial mixing in the plumes. The experimentally derived rate constant for the oxidation of Fe(II) by dioxygen is on the order of $10^2\ M^{-1} \cdot s^{-1}$ under the solution conditions interrogated in this study (4, 7). The absence of detectable Fe(III) species was consistent with the forward reaction (Eq. **4**) and rapid production of superoxide (Eq. **1**) following reduction of superoxide by Mn(II) (25) or sulfide (26). Within 0.5 m of the Q-vent orifice (∼25 °C), the maximum O_2 concentration (and thus H_2O_2 that

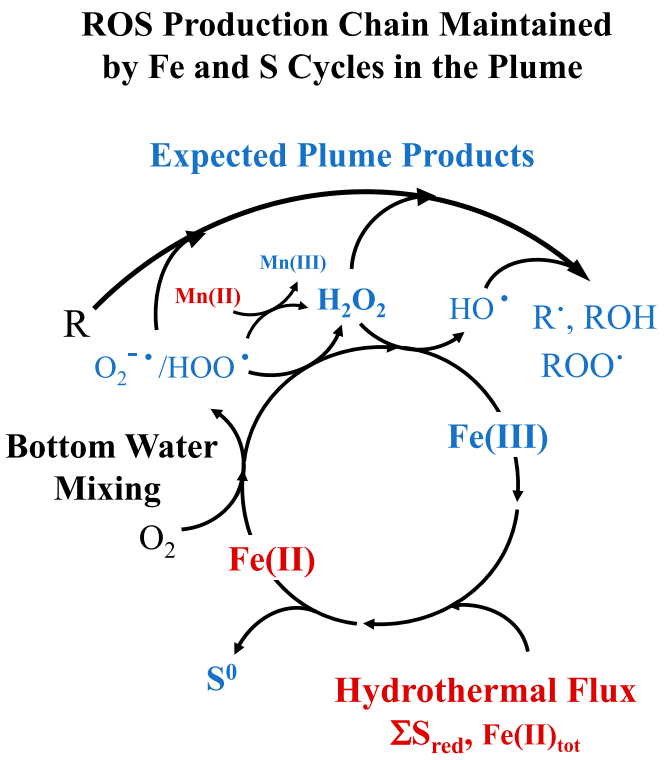

Fig. 2. The intersections between the Fe, S, and ROS cycles. The coinjection of reduced Fe and S species from vents into oxic bottom water generates plumes that support extended ROS generation in the deep ocean, enabling cooxidation of other dissolved species. R = ambient molecular species, for example, DOC. Red indicates hydrothermal inputs, blue indicates plume products, and bold indicates measured species. Black indicates bottom-water species.

could be produced) was predicted to be 39 μM based on Eqs. **1** and **2** and the mixing of seawater with plume water (Eq. **7**). However, the H_2O_2 was about 2 μM, consistent with the rapid reaction with ambient Fe(II) (1) and other reductants in the plume [e.g., H_2S and S(0)]. As temperature decreased to 2 °C, the measured H_2O_2 concentration increased as available reductants decreased in concentration (H_2O_2 production became greater than consumption), and reactions were slowed. The instantaneous concentration of H_2O_2 measured could easily have been maintained by the cyclic oxidation of measured Fe(II)- or Mn(II)-containing species (Eqs. **2** and **6**) (25) in conjunction with ambient sulfur species (Eq. **5**) (6, 7, 26). Eq. **5** predicted a similar trend for H_2O_2 and S^0 production in the plume. The concentration of S^0 was measured at several sites during the cruise (23) but only overlapped with ROS sampling during dive 4890 and only at biovent. The range of S^0 concentrations in the Biovent plume was 1 to 19 μM (23), very close to the range of the measured H_2O_2 for that dive (2.2 to 5.8 μM, Table 1). While Fe(III) was the likely oxidant for H_2S in the plume, the absence of detectable Fe(III) in the recovered plume water was expected where an excess of H_2S would sustain the Fe(II) cycles (Eq. **4**) (6, 7, 12, 23). These results were consistent with coupling of the Fe and S cycles in support of ROS production as depicted in Fig. 2.

An estimate of the efficiency of H_2O_2 production during metal-mediated sulfide oxidation in plumes was derived from the slope of the correlation for the initial O_2 input and measured H_2O_2 from Fig. 4. The slope of the correlation yielded a predicted production efficiency of ~6.5% on a mole/mole basis, indicating the intensity of consumption reactions for O_2 and/or H_2O_2 during initial plume mixing. The negative intercept for H_2O_2 was consistent with the short lifetime of H_2O_2 under plume conditions

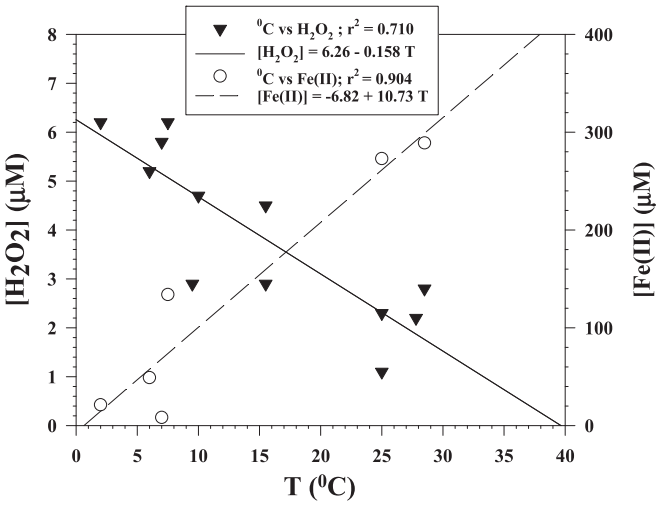

Fig. 3. [Fe(II)] and [H_2O_2] versus temperature of the plume waters for both vent sites where samples were taken. Note the positive correlation for [Fe(II)] and the negative correlation for [H_2O_2].

that resulted in an underprediction of the efficiency of the ROS chain propagation. However, even at 6.5% production efficiency, the reduction of O_2 by reduced vent species [e.g., sulfide and Fe(II)] accounted for a major source of H_2O_2 to the deep ocean. Subsequent reduction of the resulting Fe(III) by excess sulfide as the plume rose would have continued to produce H_2O_2 and, at the measured pH range of the plume (Table 1), the more reactive hydroxyl radical (Eq. **3**) (1, 5–7, 25–28).

Hydroxyl radical is an unselective oxidant that can be reduced by organic and inorganic species often at nearly diffusion-controlled rates. Two factors may be critical to the impact of hydroxyl radical production in plume waters on DOC lifetimes: the intensity of ROS production and the fraction of that production available for reactions with DOC. The intensity of ROS

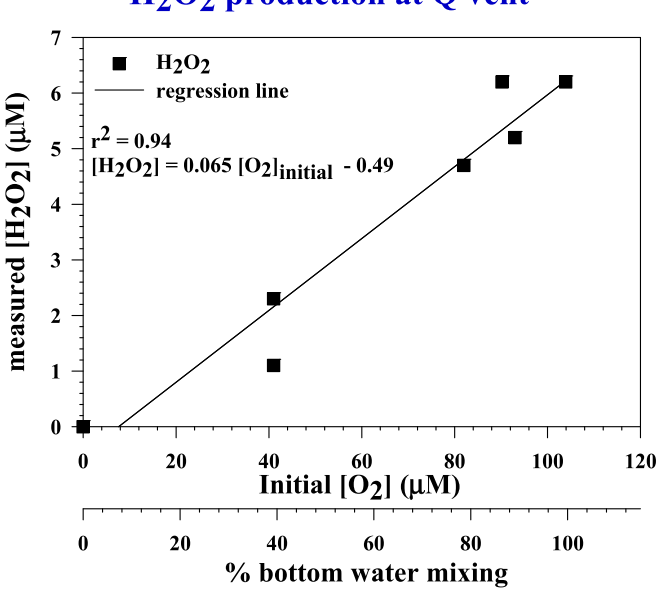

Fig. 4. Initial [O_2] in the Q-vent plume waters was calculated from mixing of vent water with bottom water using temperature as a conservative parameter. The high correlation indicates production of H_2O_2 in the plume. The vent fluid endmember (40 °C) was plotted assuming [H_2O_2] and [O_2] = 0 μM.

production was demonstrated by the measured inventory of H_2O_2 that was maintained, despite the high concentrations of potential reactive sinks in the plume [i.e., Fe(II) and HS^-]. The relative rates of reaction with Fe(II) ($k = 1{,}660\ M^{-1} \cdot s^{-1}$) (5) versus HS^- ($k = 82\ M^{-1} \cdot s^{-1}$) (29) at the median pH of our samples (pH 6) in the oxygen-depleted plume confirmed that the production of hydroxyl radical via the Fenton reaction was the dominant sink for H_2O_2. A parallel first order kinetic model developed for batch reactors (30) was applied to estimate the fraction of hydroxyl radical that remained available for reaction with ambient DOC. The model developed for the current study was based on the measured and estimated concentrations of reducing materials in the vent region that were known to react with hydroxyl radicals (reference *SI Appendix* for model details). The model predicted that as much as 1.6% of the hydroxyl radical would have been available to react with ambient DOC under the high-temperature conditions observed during initial mixing. The fraction fell to 0.67% under conditions observed further up the plume and 0.36% for ambient seawater. The model was also run for a surface freshwater model DOC fraction for comparison. The fraction fell from 0.36 to 0.15% under plume conditions for the surface model DOC. However, the efficiency of the process for either model DOC is within an order of magnitude of that typically observed in technological systems engineered for hydroxyl radical production: for example, O_3/H_2O_2 systems built for wastewater treatment (30). The model indicated that the concentration of bromide was a critical factor for determining the availability of hydroxyl radical for reacting with DOC. The low concentration of bromide in hydrothermal plumes relative to seawater indicated that hydroxyl radical would be more important for DOC oxidation in the plume environment than would be expected in the open water column. Furthermore, the locally high-ROS production intensity in this continuous flow-through system is likely to make this a significant mechanism of hydroxyl radical reaction with DOC in the ocean.

Global Estimate of Hydrothermal ROS Production. The estimated reaction efficiency from Fig. 4 provided an approximation of the impact of the reoxidation of the global hydrothermal sulfide flux as ROS production. The reaction efficiency from Fig. 4 suggests that at least 6.5% of the hydrothermal H_2S flux would yield H_2O_2. This is a minimum estimate of the ROS production and neglects consumption in the high-temperature plume. The further oxidation of S^0 to sulfate could result in even higher-ROS yields, but the more conservative reaction efficiency was assumed here. Murphy et al. (6) predicted that from 5 to 50% of the reoxidation of microbially produced sulfide could lead to ROS production based on laboratory studies of model systems. The estimated production efficiency in plumes is in agreement with the low end of the range for the laboratory results. Given that the global vent flux of reduced S species is on the same order as that generated through microbially mediated sulfate reduction (9, 10, 31, 32), plume ROS production (as hydrogen peroxide) is important in maintaining the global ROS inventory.

The production of ROS in plumes can speculatively be scaled based on the input of reduced sulfur from ridges and ridge flanks that is on the order of 10^{13} moles S/y (9, 10), similar to global microbial sulfate reduction (31). Based on the estimated 6.5% efficiency of the chain reaction leading to H_2O_2 production, the observed process is expected to lead to global production of ROS on the order of 0.7×10^{12} moles ROS/y (as H_2O_2). This is consistent with a separate estimate of 0.2 to 1.2×10^{12} moles ROS/y that results from simply multiplying the plume water flux of $\sim 2 \times 10^{17}$ L/y (9, 10) by the range of measured H_2O_2 concentration from this study. The potential impact of plume-derived ROS on the global ROS budget can be scaled against the estimated 1 to 10×10^{12} moles H_2O_2/y generated by photochemical processes (3, 7). This preliminary study documents hydrothermally derived ROS and the initial comparison it affords suggests these nonphotochemical sources of ROS may be comparable in magnitude to surface waters. Given the relative spatial heterogeneity of plume sources, the local intensity of ROS cycling adjacent to hydrothermal vents may be among the highest yet measured in a natural system.

Implications with Respect to the Global C Cycle. The oceanic carbon reservoir, as refractory DOC, is on the same order of the carbon reservoir (as CO_2) in the atmosphere, and processes that mediate the mineralization of DOC to CO_2 are critical to the global carbon cycle. While it has been proposed that the oceanic inventory of refractory DOC is controlled by photochemical degradation in surface waters (33), the deep refractory pool of DOC (>1,000 m) is less photochemically reactive than shallower material (34). Photochemically mediated production of ROS leads to near-surface ocean enrichments of hydrogen peroxide in the 20 to 80 nanomolar range (35) and may contribute to the mineralization of DOC fractions via photo-Fenton reactions (1, 3, 34). However, the abundance of these species is low compared to that measured in hydrothermal plumes, and ambient surface ocean pH (~8) is less favorable to production of the more reactive ROS, hydroxyl radical. In contrast, high–hydrogen peroxide concentrations and the lower-pH values observed in plumes are more consistent with much more reactive natural systems like cloudwaters (36) and engineered systems (30). The depleted DOC inventory of about 14 μM measured previously in the high-temperature plume at the EPR (18) is consistent with the hydrothermal alteration/decomposition of nonaromatic compounds (37) during hydrothermal circulation. The observed increase in hydroxylated aromatic compounds in plumes from this and other vent locations (18, 38, 39) suggest that this abiotic oxidation process is not unique to this hydrothermal system and is related to the high intensity of hydroxyl radical production and reactivity reported here. Overall, the measured chemical inventories of ROS in plumes indicate an efficient flow-through reactor for refractory DOC in the oceans.

In summary, hydrothermal plumes represent a source of ROS to the deep ocean. The measured H_2O_2 production, pH values, and abundant reduced S and Fe species in plumes indicated conditions likely to result in significant ROS production, as H_2O_2, under conditions likely to support hydroxyl radical production as well (25, 26). Hydroxyl radical reacts with organic molecules at essentially diffusion-controlled rates (26) making plumes a possible sink for even the most refractory DOC and POC in the deep ocean. Oxidized derivatives of benzoic acid (2,3-dihydroxybenzoic acid, a catechol, and 4-hydroxybenzoic acid) and the organic sulfur compound 2,3-dihydroxypropane-1-sulfonate have been reported in plumes (18) as have increases in O/C ratios and polyphenolic compounds (38), all circumstantial evidence for a role for ROS in the fate of refractory carbon. The hydrothermal ROS production estimated here would have a major impact on the oceans DOC inventory. In this context, it is not surprising that the measured ages of DOC in the deep ocean (40, 41) are on the same order as the estimates for the circulation time of the ocean through vent plumes (14).

Materials and Methods

Plume and Diffuse Flow Sampling. The vent fields at 9 North on the EPR were accessed with the human-occupied submersible *Alvin*. Water samples from plumes and a diffuse flow area were collected with 1/8-inch or 3.175-mm Teflon tubing housed in a delrin wand that could be positioned by a manipulator from *Alvin*. Samples were collected in syringes set in a modified Jahnke syringe sampler (21) that was remotely triggered. The wand above also housed Au/Hg working electrodes, which were cabled to the electrochemical analyzer (see below). The Teflon tubing was attached to the cable and connected to the syringe sampler in the *Alvin* basket. Syringe samplers were set up in pairs with one of the pair for water collection for shipboard analysis of Fe and Mn species and the second of the pair preloaded with reagents for production of a hydrogen peroxide signal.

Hydrogen Peroxide Measurement. Hydrogen peroxide concentrations in plume samples were analyzed by the peroxidase-catalyzed conversion of amplex red to resorufin (20, 42). Reagent solutions were made up daily from preweighed frozen solid for HRP and preweighed salts for buffers. Amplex red solution was made up from premeasured vials containing stock 10-acetyl-3,7-dihydroxyphenoxazine dissolved in DMSO. While the precision of the measurements was better than 5%, procedural blanks varied considerably with variations in shipboard deionized (DI) water quality, typically ranging from 50 to 100 nM. This was probably associated with the ultraviolet (UV) disinfection system used for the water supply. The worst-case result from these measurements was used to estimate a conservative minimum detection limit (MDL) of 200 nM for the shipboard results.

Water samples were drawn into 35-mL syringes that were precharged with 8 mL of a mixture of HRP at an activity of 0.4 U/mL and amplex red at a concentration of 100 μM in 0.05 M Phosphate buffer (>200-fold excess to the reduced Fe and S measured in the samples) made up in prefiltered seawater adjusted to pH 7.4. Thus, Fe(III) binding to phosphate was much faster than the reaction of Fe(III) with H_2S, limiting the impact of the possible interferent. Reagent concentrations were previously validated for systems containing high Fe(II) and sulfide loading (>500 μM) (6, 7) to insure no signal suppression of the analyte signal associated with ambient sulfide (43). As we use 100 μM amplex red to keep the S(−2)/amplex red ratio to below 1 to 2, sulfide does not interfere, and we achieve 90 to 100% efficiency for the reaction of H_2O_2 to form resorufin as also found by Wang et al. (43), who worked at lower-sulfide concentrations. The phosphate buffer served to shut down the reformation and oxidation of FeS species by sequestering Fe(III) to, as near as possible, capture an instantaneous measure of ROS inventories in the plume. The initial concentrations of amplex red and HRP were sufficiently high to out compete the reaction of hydrogen peroxide with ambient reduced Fe and Mn by at least two orders of magnitude (42). Charged syringes with either prefiltered seawater and/or shipboard DI water were prepared as procedural blanks concurrent with the preparation of the syringe samplers. The blank syringes during the *Alvin* dive were analyzed with the recovered samples. The resultant blank measurements were not different from reagent blanks using shipboard DI water (see the previous paragraph). The persistence of HRP activity was confirmed on procedural blanks that were carried in syringes for the duration of a dive and spiked with H_2O_2 upon return to the ship.

Cyclic Voltammetry Measurements. A DLK-SUB IV electrochemical analyzer from Analytical Instrument Systems, Inc. was used to collect O_2 and H_2S data (22). Briefly, this instrument contained a potentiostat, a multiplexer (to monitor up to four solid-state Au amalgam [Au/Hg] working electrodes one at a time), and a computer, which communicated with another computer in the *Alvin*. The electronics were enclosed in a titanium housing and powered via a cable from *Alvin.* A Delrin wand housed the Au/Hg-working electrodes, which were cabled to the analyzer, and 1/8-inch Teflon tubing, which allowed sampling via the syringe sampler. The wand was positioned by a manipulator from *Alvin*; the solid-state Ag/AgCl reference and Pt counter electrodes were placed on the *Alvin* basket at 1.6 °C in order to keep their temperature constant. The wand was positioned by a manipulator from *Alvin*. For each discrete location sampled by syringe, 5 to 7 voltammetric scans were taken and the data averaged. The potential range scanned was −0.1 to −1.8 V to −0.1 V at a scan rate of 2,000 mV · s^{-1}. A 5-s conditioning step at −0.9 V and another at −0.1 V for 2 s was applied before each scan to electrochemically clean the Hg surface. The minimum detectable limits for free sulfide (Σ [H_2S] and [HS^-]) and O_2 are 0.2 and 3 μM, respectively.

Lastly, the in situ voltammetry system did not detect thiosulfate (MDL, 10 μM) or polysulfides (MDL, 0.2 μM). Electrodes were calibrated before and after each *Alvin* dive to ensure data reliability.

Fe and Mn Speciation Measurements. Six samples noted in Table 1 were processed for soluble Fe and Mn speciation following collection using the syringe system described above without any preloaded reagents or buffer. Samples were collected within the rising plume of active vents. Syringe samples were filtered immediately upon arrival on deck using 0.2-μm Luer-lock syringe filters. Filtrate was collected into acid, washed, and DI rinsed 50-mL Falcon tubes.

The Fe(II) concentration was determined after the addition of Ferrozine reagent and analyzed spectrophotometrically based on absorbance at 562 nm (44). Another aliquot of sample was treated with hydroxylamine to measure total Fe and calculate Fe(III) by difference in the samples, but no Fe(III) was detected in the filtrate (MDL is 100 nM).

The Mn speciation of the filtrate was analyzed spectrophotometrically at 468 nm by the addition of a soluble porphyrin ligand (24). In this method, a porphyrin–Cd complex undergoes a rapid metal substitution reaction with Mn(II) in the sample, whereas weak Mn(III)–L complexes undergo a slow ligand substitution reaction. Using the known reaction rate constant "k_1" for the reaction with Mn(II) in a sample completely reduced with hydroxylamine, "k_2," the rate constant for the Mn(III)–L ligand substitution reaction, could be obtained and, subsequently, the concentration of each Mn species was determined in the sample. The differential kinetics of the reaction of Mn(II) and weak Mn(III)–L complexes with the added porphyrin were observed over 15 min using a quartz 1-cm cell in an ultraviolet-visible diode array spectrophotometer coupled with Olis Globalworks software, but weak Mn(III)–L complexes (MDL is 50 nM) were not detected. Samples were also amended with hydroxylamine to assess the presence of strong Mn(III)–L complexes (not outcompeted by added porphyrin), and only strong Mn(III)–L complexes were detected (MDL is 50 nM).

Data Availability. The Earth and space sciences data are deposited in the rolling deck to repository data base (R2R) https://www.rvdata.us/search/cruise/AT37-11. All other study data are included in the article and/or *SI Appendix*.

ACKNOWLEDGMENTS. This work was supported by the Department of Chemistry and Biochemistry at University of South Carolina, the School of Marine Science & Policy at University of Delaware, and the NSF through CO OCE-1559274 and CHE-1308801 to T.J.S. and CO OCE-1558738 and MGG OCE-1558712 to G.W.L.III. Kathryn Shaw completed the artwork for Fig. 1. We thank the *Alvin* group, which is part of the National Deep Submergence Facility at Woods Hole Oceanographic Institution, and the captain and crew of the research vessel *Atlantis* for their support in all aspects of our research. We also thank the guest editor and two anonymous reviewers for comments and suggestions that have improved this manuscript.

1. R. G. Zepp, B. C. Faust, J. Hoigne, Hydroxyl radical formation in aqueous reactions (pH 3-8) of iron(II) with hydrogen peroxide: The photo-Fenton reaction. *Environ. Sci. Technol.* **26**, 313–319 (1992).
2. L. C. Powers, W. L. Miller, Blending remote sensing data products to estimate photochemical production of hydrogen peroxide and superoxide in the surface ocean. *Environ. Sci. Process. Impacts* **16**, 792–806 (2014).
3. Y. Chen *et al*., Prediction of photochemically produced reactive intermediates in surface waters via satellite remote sensing. *Environ. Sci. Technol.* **54**, 6671–6681 (2020).
4. F. J. Millero, S. Sotolongo, M. Izaguirre, The oxidation-kinetics of Fe(II) in seawater. *Geochim. Cosmochim. Acta* **51**, 793–801 (1987).
5. F. J. Millero, S. Sotolongo, The oxidation of Fe(II) with H_2O_2 in seawater. *Geochim. Cosmochim. Acta* **53**, 1867–1873 (1989).
6. S. A. Murphy *et al*., Geochemical production of reactive oxygen species from biogeochemically reduced Fe. *Environ. Sci. Technol.* **48**, 3815–3821 (2014).
7. S. A. Murphy *et al*., Hydrous ferric oxides in sediment catalyze formation of reactive oxygen species during sulfide oxidation. *Front. Mar. Sci.* **3**, 227 (2016).
8. D. M. C. Dias *et al*., Production of reactive oxygen species in the rhizosphere of a spartina-dominated salt marsh systems. *Aquat. Geochem.* **22**, 573–591 (2016).
9. H. Elderfield, A. Schultz, Mid-ocean ridge hydrothermal fluxes and the chemical composition of the ocean. *Annu. Rev. Earth Planet. Sci.* **24**, 191–224 (1996).
10. D. J. Kadko, D. J. Baross, J. Alt, "Hydrothermal fluxes and global change" in *Seafloor Hydrothermal Systems: Physical, Chemical, Biological, and Geological Interactions*, S. E. Humphris, R. A. Zierenberg, L. S. Mullineaux, R. E. Thomson, Eds. (American Geophysical Union, 1995), pp. 446–466.
11. C. von Sonntag, H.-P. Schuchmann, The elucidation of peroxyl radical reactions in aqueous solution with the help of radiation-chemical methods. *Angew. Chem. Int. Ed. Engl.* **30**, 1229–1253 (1991).
12. G. W. Luther III, The role of one- and two-electron transfer reactions in forming thermodynamically unstable intermediates as barriers in multi-electron redox reactions. *Aquat. Geochem.* **16**, 395–420 (2010).
13. G. W. Luther III, *Inorganic Chemistry for Geochemistry and Environmental Sciences: Fundamentals and Applications* (John Wiley and Sons Inc., 2016).
14. C. R. German *et al*., Hydrothermal impacts on trace element and isotope ocean biogeochemistry. *Philos. Trans.- Royal Soc., Math. Phys. Eng. Sci.* **374**, 20160035 (2016).
15. C. R. German, K. L. Von Damm, "Hydrothermal processes" in *Treatise on Geochemistry*, H. D. Holland, K. K. Turekian, Eds. (Elsevier, 2003), pp. 181–222.
16. J. M. Edmond *et al*., Ridge crest hydrothermal activity and the balances of the major and minor elements in the ocean: The Galapagos data. *Earth Planet. Sci. Lett.* **46**, 1–18 (1979).
17. A. J. Findlay *et al*., Distribution and size fractionation of elemental sulfur in aqueous environments: The Chesapeake Bay and Mid-Atlantic Ridge. *Geochim. Cosmochim. Acta* **142**, 334–348 (2014).
18. K. Longnecker, S. M. Sievert, S. P. Sylva, J. S. Seewald, E. B. Kujawinski, Dissolved organic carbon compounds in deep-sea hydrothermal vent fluids from the East Pacific Rise at 9°50′N. *Org. Geochem.* **125**, 41–49 (2018).

19. K. L. Roe, R. J. Schneider, C. M. Hansel, B. M. Voelker, Measurement of dark, particle-generated superoxide and hydrogen peroxide production and decay in the subtropical and temperate North Pacific Ocean. *Deep Sea Res. Part I Oceanogr. Res. Pap.* **107**, 59–69 (2016).
20. M. Zhou, Z. Diwu, N. Panchuk-Voloshina, R. P. Haugland, A stable nonfluorescent derivative of resorufin for the fluorometric determination of trace hydrogen peroxide: Applications in detecting the activity of phagocyte NADPH oxidase and other oxidases. *Anal. Biochem.* **253**, 162–168 (1997).
21. R. A. Jahnke, M. B. Christiansen, A free-vehicle benthic chamber instrument for sea floor studies. *Deep-Sea Res.* **36**, 625–637 (1989).
22. G. W. Luther III *et al*., Use of voltammetric solid-state (micro)electrodes for studying biogeochemical processes: Laboratory measurements to real time measurements with an in situ electrochemical analyzer (ISEA). *Mar. Chem.* **108**, 221–235 (2008).
23. A. J. Findlay *et al*., Iron and sulfide nanoparticle formation and transport in nascent hydrothermal vent plumes. *Nat. Comm.* **10**, 1597 (2019).
24. V. E. Oldham, M. R. Jones, B. M. Tebo, G. W. Luther III, Oxidative and reductive processes contributing to manganese cycling at oxic-anoxic interfaces. *Mar. Chem.* **195**, 122–128 (2017).
25. B. H. J. Bielski, D. E. Cabelli, R. L. Arudi, A. B. Ross, Reactivity of HO_2/O_2^- radicals in aqueous solution. *J. Phys. Chem. Ref. Data* **14**, 1041–1100 (1985).
26. J. M. Burns, P. S. Craig, T. J. Shaw, J. L. Ferry, Multivariate examination of Fe(II)/Fe(III) cycling and consequent hydroxyl radical generation. *Environ. Sci. Technol.* **44**, 7226–7231 (2010).
27. M. A. A. Schoonen, A. D. Harrington, R. Laffers, D. R. Strongin, Role of hydrogen peroxide and hydroxyl radical in pyrite oxidation by molecular oxygen. *Geochim. Cosmochim. Acta* **74**, 4971–4987 (2010).
28. E. Rickard *et al*., FeS-induced radical formation and its effect on plasmid DNA. *Aquat. Geochem.* **17**, 545–566 (2011).
29. F. J. Millero, A. LeFerriere, M. Fernandez, S. Hubinger, J. P. Hershey, Oxidation of hydrogen sulfide with hydrogen peroxide in natural waters. *Environ. Sci. Technol.* **23**, 209–213 (1989).
30. W. H. Glaze, J. W. Kang, Advanced oxidation processes. Test of a kinetic model for the oxidation of organic compounds with ozone and hydrogen peroxide in a semibatch reactor. *Ind. Eng. Chem. Res.* **28**, 1580–1587 (1989).
31. M. W. Bowles, J. M. Mogollón, S. Kasten, M. Zabel, K. U. Hinrichs, Global rates of marine sulfate reduction and implications for sub-sea-floor metabolic activities. *Science* **344**, 889–891 (2014).
32. S. H. Bottrell, R. J. Newton, Reconstruction of changes in global sulfur cycling from marine sulfate isotopes. *Earth Sci. Rev.* **75**, 59–83 (2006).
33. K. Mopper *et al*., Photochemical degradation of dissolved organic carbon and its impact on the oceanic carbon cycle. *Nature* **353**, 60–62 (1991).
34. L. Powers, L. C. Babcock-Adams, J. K. Enright, W. L. Miller, Probing the photochemical reactivity of deep ocean refractory carbon (DORC): Lessons from hydrogen peroxide and superoxide kinetics. *Mar. Chem.* **177**, 306–317 (2015).
35. J. Yuan, A. M. Shiller, The distribution of hydrogen peroxide in the southern and central Atlantic ocean. *Deep Sea Res. Part II Top. Stud. Oceanogr.* **48**, 2947–2970 (2001).
36. C. Anastasio, B. C. Faust, J. M. Allen, Aqueous phase photochemical formation of hydrogen peroxide in authentic cloud waters. *J. Geophys. Res.* **99**, 8231–8248 (1994).
37. T. M. McCollom, J. S. Seewald, B. R. T. Simoneit, Reactivity of monocyclic aromatic compounds under hydrothermal conditions. *Geochim. Cosmochim. Acta* **65**, 455–468 (2001).
38. P. E. Rossel *et al*., Thermally altered marine dissolved organic matter in hydrothermal fluids. *Org. Geochem.* **110**, 73–86 (2017).
39. H.-T. Lin, D. J. Repeta, L. Xu, M. S. Rappée, Dissolved organic carbon in basalt-hosted deep subseafloor fluids of the Juan de Fuca Ridge flank. *Earth Planet. Sci. Lett.* **513**, 156–165 (2019).
40. E. R. M. Druffel, S. Griffin, A. I. Coppola, B. D. Walker, Radiocarbon in dissolved organic carbon of the Atlantic Ocean. *Geophys. Res. Lett.* **43**, 5279–5286 (2016).
41. S. K. Bercovici *et al*., Aging and molecular changes of dissolved organic matter between two deep oceanic end-members. *Global Biogeochem. Cycles* **32**, 1449–1456 (2018).
42. J. N. Rodríguez-López *et al*., Mechanism of reaction of hydrogen peroxide with horseradish peroxidase: Identification of intermediates in the catalytic cycle. *J. Am. Chem. Soc.* **123**, 11838–11847 (2001).
43. N. Wang, C. J. Miller, P. Wang, T. D. Waite, Quantitative determination of trace hydrogen peroxide in the presence of sulfide using the Amplex Red/horseradish peroxidase assay. *Anal. Chim. Acta* **963**, 61–67 (2017).
44. L. L. Stookey, Ferrozine-a new spectrophotometric reagent for iron. *Anal. Chem.* **42**, 779–781 (1970).